Measurement of static friction in mechanical couplings of articulated microrobots

Richard Yeh, Kristofer S. J. Pister

University of California at Los Angeles
Dept. of Electrical Engineering, Engineering IV, 54-148
Los Angeles, CA 90095-1594

ABSTRACT

Force measurements from three dimensional polysilicon mechanisms under various loading conditions are presented. Force was measured using the deflection of polysilicon spring gauges with known dimensions and estimated elastic properties. Force measurements were made to determine the force required to overcome static friction when rotating hinged structures with and without external loading using a sliding mechanism. Both loaded and unloaded mechanisms display a wide statistical variation in friction force. Unloaded mechanisms require on average 1-5μN of force to move, whereas mechanisms manipulating 3.5μN loads require on average 1-10μN of force. These measurements are motivated by an effort to produce articulated microrobots, and progress in this area is also discussed.

Keywords: friction, microrobots, microhinges, mechanical couplings, lever arms, shuttles, robot links.

1. INTRODUCTION

Living insects can be a source of great inspiration in the development of microrobots. The insect has articulated joints and linkages made from rigid exoskeleton. Although they have a limited intelligence, they are arguably the most successful species in terms of survival. To mimic nature's example of "microrobots," work has begun to create MEMS articulated structures[1,2,3]. Using polysilicon microhinges[4], rigid links can be created by folding thin-film polysilicon plates into a hollow triangular beam (HTB). Hinges can also be used as revolute joints between rigid links to create articulated structures. Figure 1a shows a diagram of our proposed articulated manipulator, which consists of rigid links connected by revolute joints. Figure 1b shows a picture of a macroscopic remote-controlled model of our manipulator with three HTB's. Figure 2 shows a SEM picture of an HTB and a lever arm, each connected to a linear stepper motor (the particular stepper motors shown are not operational).

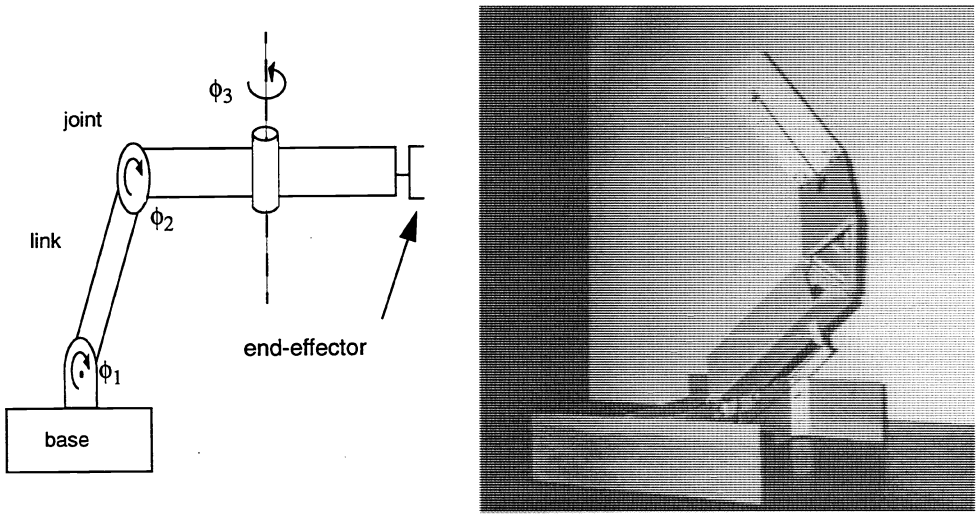

Fig. 1. Robot manipulator. (a) Structure of an articulated manipulator with revolute joints and mechanical links. (b) Photograph of an operational macroscopic articulated manipulator.

0-8194-2008-5/95/$6.00

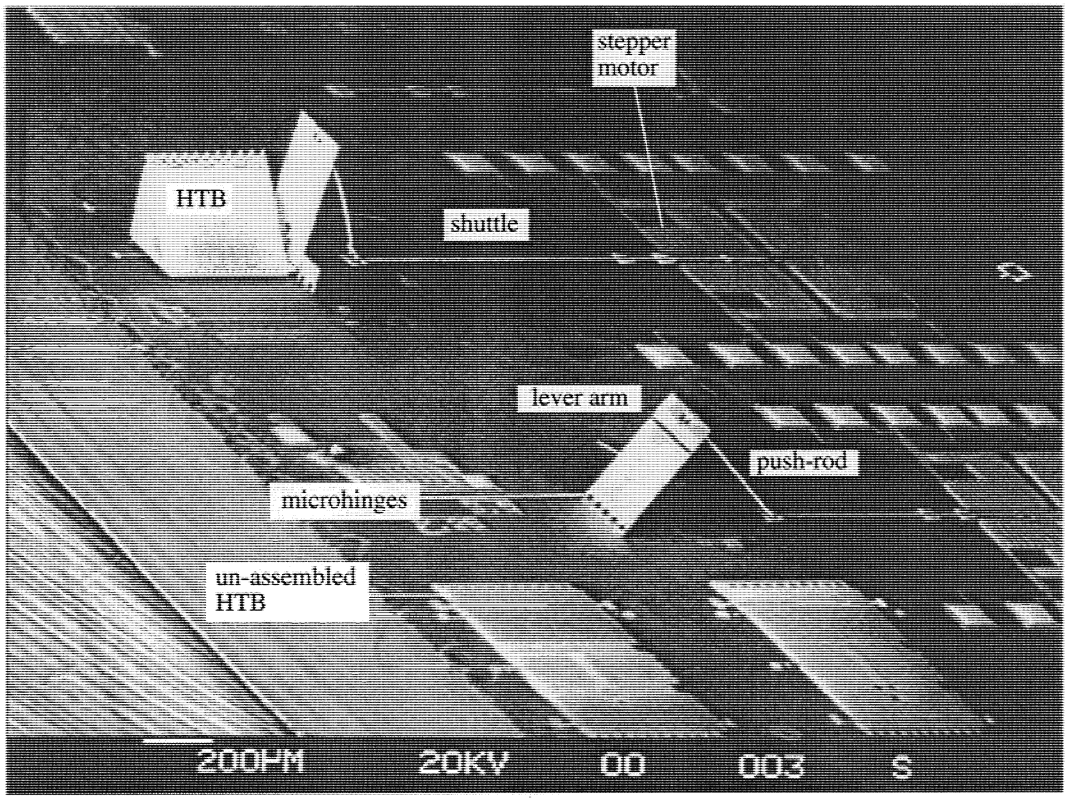

Fig. 2. SEM picture of 1-DOF robotic test structures.

To link articulated structures to actuators on the substrate, we have created mechanical couplings from polysilicon beams, plates, and hinges. To provide large linear displacements necessary in robotics systems, sliders are used rather than compliant structures. In such systems where one surface slides against another, friction is an important factor. Since typical MEMS devices have masses on the order of a few micrograms (a few tens of nanonewtons of weight), friction is often the dominating force rather than inertia.

Many papers have been published on friction between typical MEMS materials such as silicon, oxide, nitride, etc.[5,6,7]. Others have reported friction between actual microstructures[8,9]. In this paper, we investigate the friction from sliding beams and microhinged structures designed for microrobotics. First, the articulated microrobot structure is described. Next, the strength of the structures are shown, by experimentation, to be indeed stronger than conventional thin-film structures. Following, some simple mechanical couplings for the microrobot structures are described. Finally, the frictional forces in the mechanical couplings are investigated through a series of experiments.

2. RIGID MICROROBOT LINKS

A surface micromachined link, made from thin film polysilicon, must be rigid enough to support the weight of its payload and also have the requisite shape to allow joints to have independent axes of rotation. HTB's have been designed and tested to satisfy these conditions. Figure 3a shows an HTB in CAD layout. The HTB is created with three plates connected with scissor hinges, which allow two plates to rotate with respect to one another. This allows us to use probe tip manipulators to fold the two side plates up and over the center plate, creating a hollow triangular beam. The two side plates have snaplocks (Fig. 3b) along the top edges to fasten the plates in position. Figure 3c shows a SEM picture of HTB's that are assembled and rotated out of the substrate.

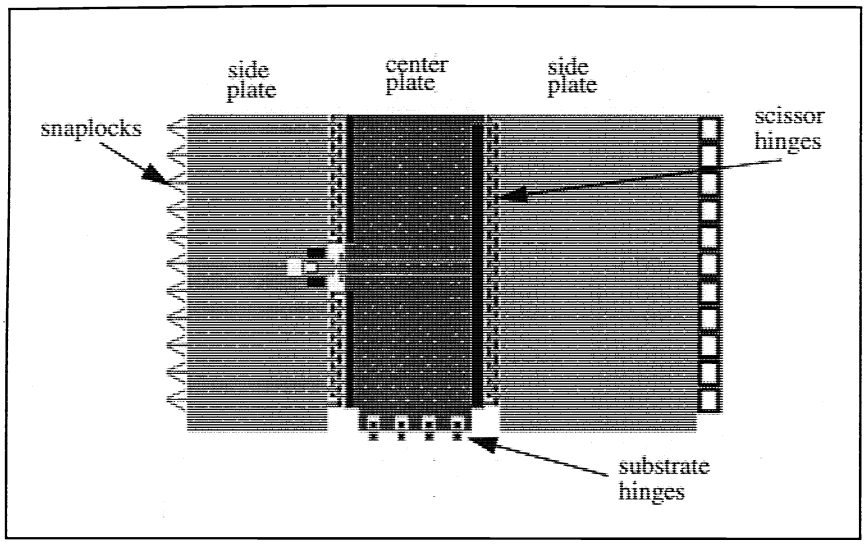

(a)

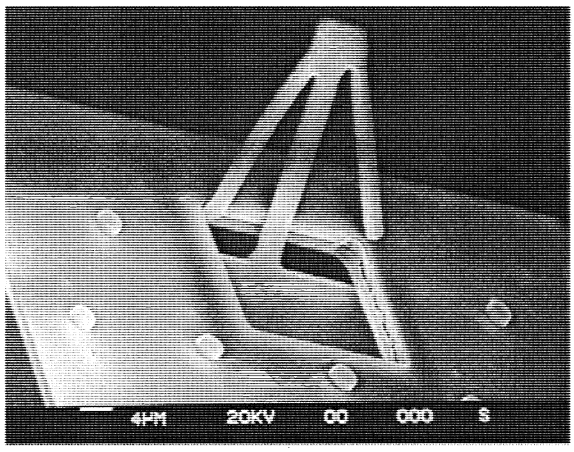

(b)

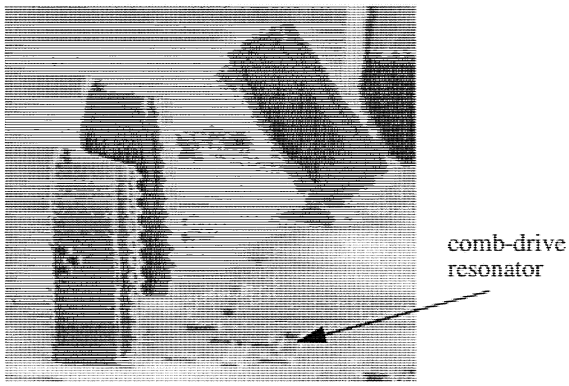

(c)

Fig. 3. HTB. (a) IC CAD layout of HTB with scissor hinges, substrate hinges, snaplocks, center plate, and side plates. This version has a right triangular cross-section. (b) SEM picture of a snaplock. (c) HTB's that are rotated from the substrate. Comb drive resonator is included for scale.

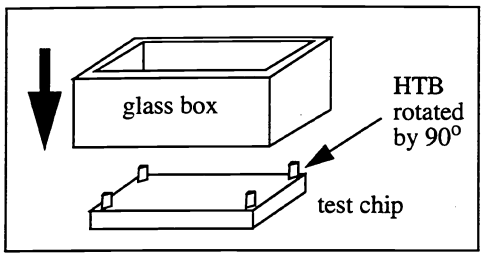

Fig. 4. Loading test on four corner HTB's.

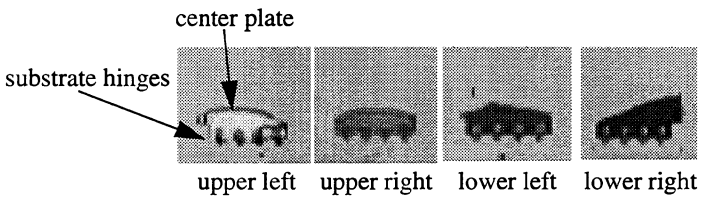

Fig. 5. Pictures of the remains of four corner HTB's after collapse.

3. STRENGTH & STIFFNESS

To find the strength of HTB's in the axial direction, a glass box was placed on top of four 432μm tall HTB's (Fig. 4) located at each corner of a $1cm^2$ die. Water was injected slowly from a syringe into the glass box until the HTB's collapsed. Videotape of the collapse indicated that when the critical load was reached, the snaplocks broke first. Next, the scissor hinges broke, freeing the side plates from the center plate. Figure 5 shows the remains of the four center plates after a loading test. All plates broke in approximately the same place, while all the substrate hinges remained intact. In three separate experiments, loads of between 8.7 and 10.2g was required to break the four HTB's. If all twelve plates that make up these four HTB's were independent, the plates would fail by buckling at a calculated total critical load of only 0.4g.

Similarly, we expect the HTB to have a higher spring constant compared to flat beams. A clamped-free flat polysilicon beam 1mm long, 100μm wide, and 2μm thick has a spring constant of approximately 0.04 N/m under small deflections. However, if we could create an HTB with rigid corners by folding 3 such plates into a tube, the spring constant would be increased to 1,400 N/m. Since in reality, the HTB does not have rigid corners due to non-ideal snaplocks and scissor hinges, we do not expect the overall stiffness of the HTB to be as high as an HTB with rigid corners. However, based on qualitative evidence so far, it appears that at least two orders of magnitude stiffness improvement has been realized. The strength of the HTB's was demonstrated when a 17mm x 8mm x 100μm glass cover slip (~330μN) was accidentally dropped by roughly 5mm on a 432μm long HTB. The force ripped the HTB off of the substrate but the HTB remained intact, supporting the glass cover slip above it

4. MECHANICAL COUPLINGS

Mechanical couplings are used to transmit the actuator force to the articulated structures. By using a sliding shuttle and push-rod, we have manually rotated structures out of the plane of the substrate. Figure 6 shows SEM photographs of lever arms and four-bar linkages created from two coupled lever arms. Each lever arm has its own push-rod and shuttle and can be manually rotated by pushing or pulling a ring at the end of the shuttle. Figure 7 shows an HTB manually rotated out of the substrate by a push-rod and shuttle. Anther way of rotating links is to use a lever arm for mechanical advantage (Fig. 8).

5. FRICTION MEASUREMENTS

To use these push-rods, shuttles, and lever arms as mechanical couplings, an actuator must be able to overcome the friction caused by the moving parts. To aid in the actuator design, we have measured the force required to actuate the mechanical couplings and articulated structures. Tests were conducted on a simple lever arm similar to the one shown in figure 6a, which consists

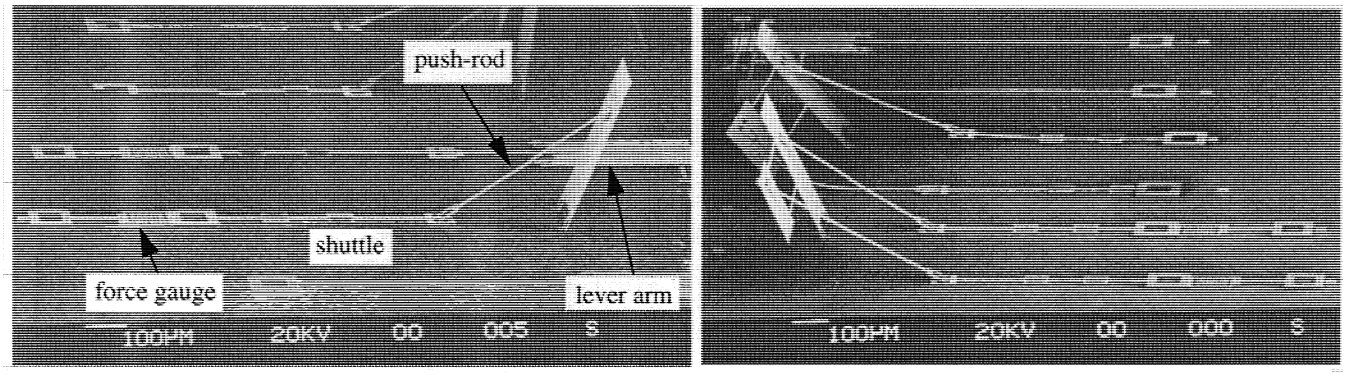

(a) (b)

Fig. 6. 1 and 2 DOF four-bar linkages. (a) SEM picture of a 1 DOF lever arm with push-rod, shuttle, and force gauge (serpentine spring). (b) SEM picture of 2 DOF coupled lever arms.

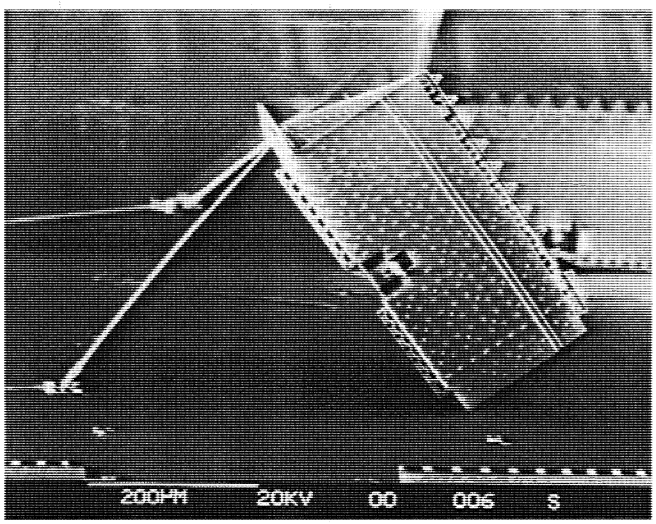

(a)

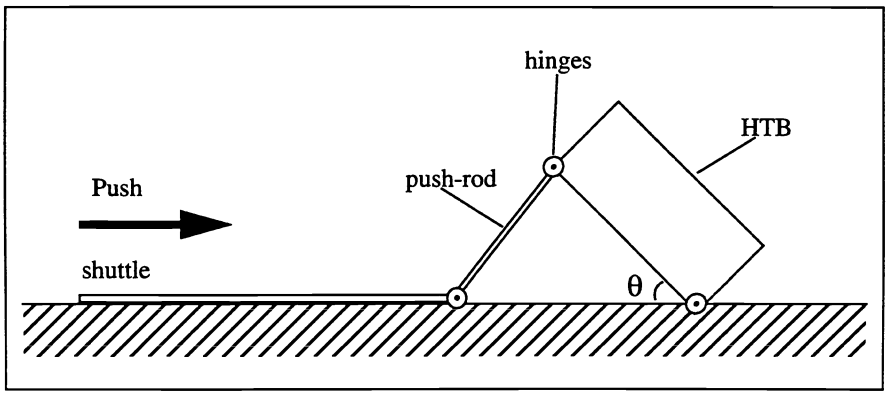

(b)

Fig. 7. (a) SEM picture of an HTB rotated with a push-rod and shuttle. (b) Diagram of the structure in (a).

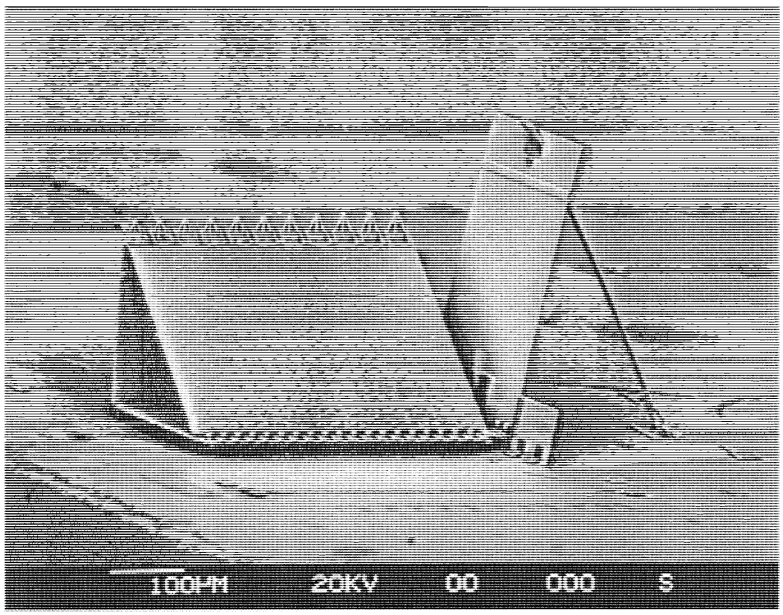

(a)

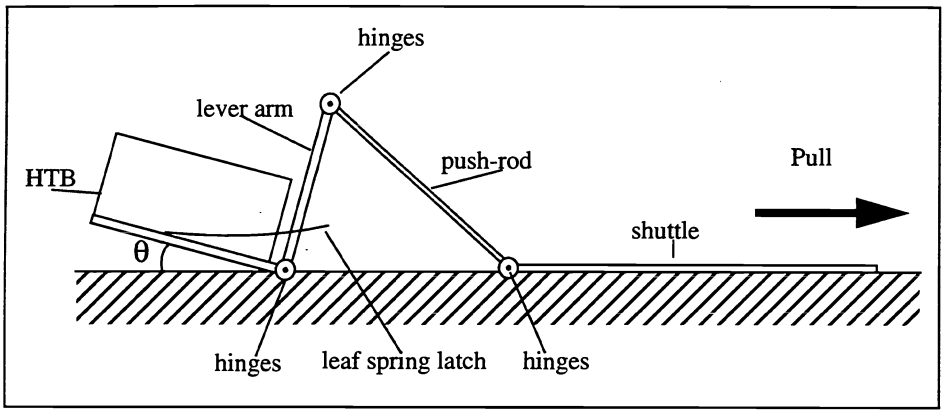

(b)

Fig. 8. (a) SEM picture of a lever arm coupled to an HTB for mechanical coupling. (b) Diagram of the structure in (a).

of a lever arm, push-rod, shuttle, and force gauge. This lever arm can be rotated from approximately 60° to 140°. Larger angles of rotation could be achieved with slight modifications to the dimensions of the lever arm components. The lever arm was slowly rotated through its range of rotation at the probe station by pulling on the serpentine-spring force gauge (Fig. 9) attached to one end of the shuttle. With our microscope/TV setup, we could resolve about 2μm of deflection. For the serpentine spring dimensions used in the experiments, the spring constant was roughly 0.4N/m of deflection, assuming a Young's modulus of 150GPa. The force gauge springs can deflect by 162μm (153μN) before failure.

5.1 Minimizing stiction

We have observed that sometimes the serpentine spring can be deflected by up to 5μm and be released and the spring would stick to the nitride surface rather than return to its original position. This occurred even on samples that were dried using the critical point method[10]. To prevent stiction from occurring during the experiments, all samples were dehydrated in an oven at 120°C for at least 20 minutes to minimize surface liquid adsorption[5]. In addition, the substrate and the probe tip used to touch the force gauge were held at the same potential to minimize electrostatic force.

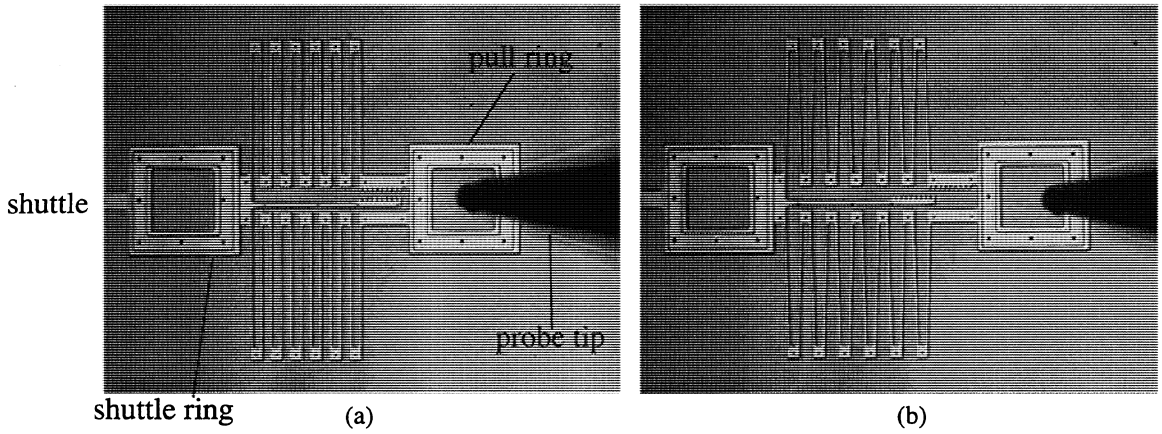

Fig. 9. A serpentine spring force gauge with two sets of 100μm x 2μm x 2μm beams. Each set has 12 beams. The spring constant is estimated at 0.4N/m. Deflections were measured visually at a magnification where 2μm can be resolved. The pull rings have a 50μm x 50μm opening for the probe tip. (a) Force gauge at rest. (b) Force gauge deflected by 28μm (11μN).

5.2 Friction on unloaded lever arms

We first measured the force required to actuate the lever arm without any load. The shuttle would slip only when sufficient force was applied to the force gauge, resulting in a jerky slipping motion. The static friction held the lever arm at any angle of rotation. The angle of rotation was roughly calculated from the position of the shuttle. Figure 10 shows the measured applied force versus the angle of rotation from 5 separate experiments. The measured force (1 to 43μN with 82% of values below 5μN) was much higher than the weight of the lever arm (~3.2nN) and the trend of the data did not resemble that of a typical torque arm system. We observed that on the average, the force required to rotate the lever arm was higher when θ is less than 90° (push-rod in tension).

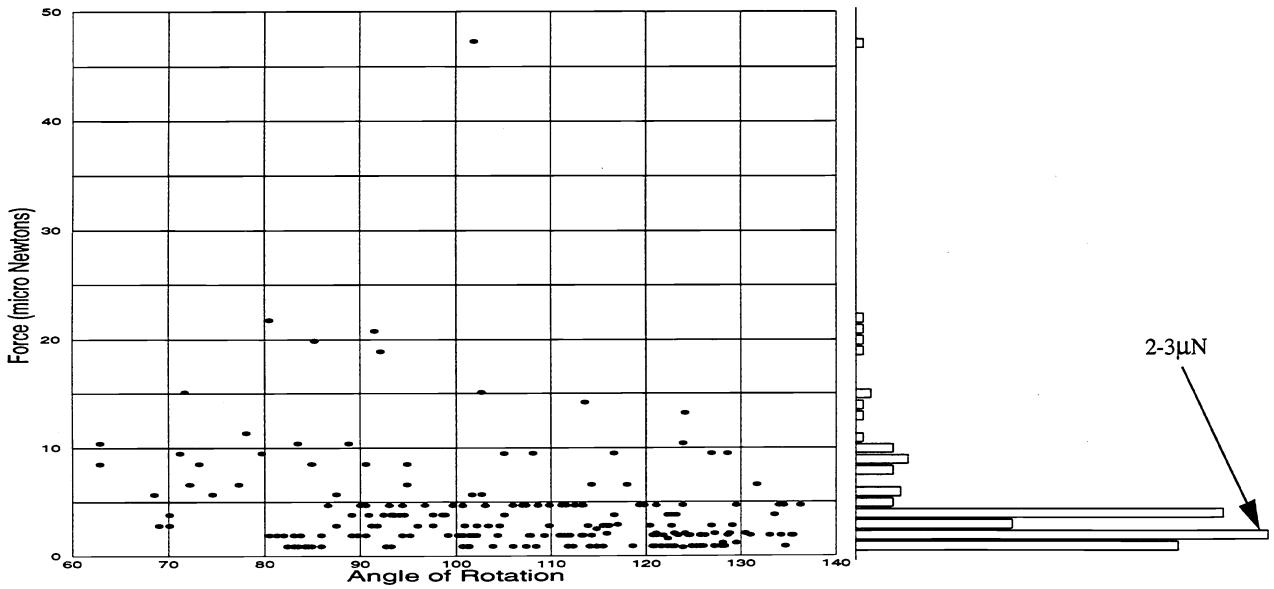

Fig. 10. Graph of force versus the angle of rotation for an unloaded lever arm system. The histogram to the right of the graph shows a peak value recurrence between 2-3μN.

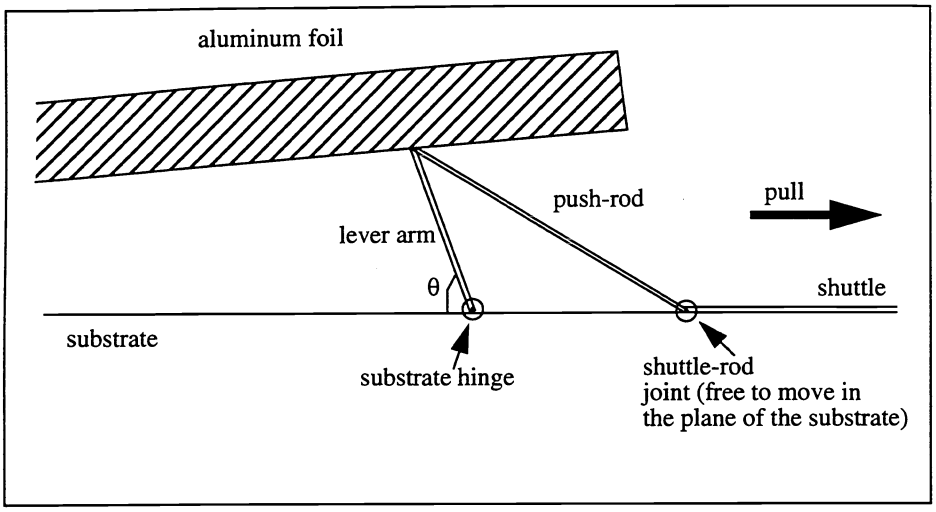

Fig. 11. Diagram of the lever arm loading test.

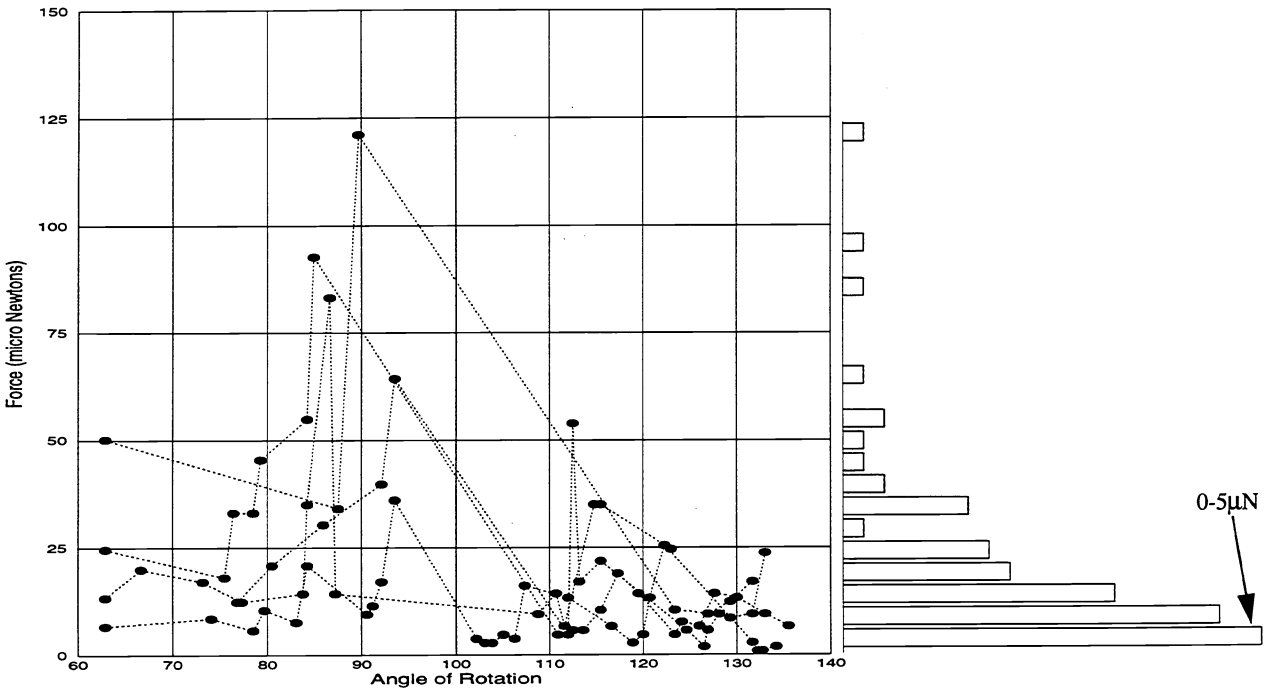

Fig. 12. Graph of force versus the angle of rotation for a lever arm system loaded with ~3.5μN of weight. The histogram to the right of the graph shows a peak value occurrence between 0-5μN.

5.3 Friction on loaded lever arms

Next, a 2.5mm x 5mm x 20μm piece of aluminum foil (~7μN of weight, half of which was supported off-chip) was placed on top of the lever arm (Fig. 11) and the test was repeated several times. The measured force versus the angle of rotation of those tests were plotted in figure 12. Again, the applied forces (1 to 120μN with 80% of the values below 25μN) were higher than that of the load and the data did not resemble that of a torque arm system. However, the data values peaked near 90°.

5.4 Buckling of the push-rod

In addition to the above tests, the buckling force of the 15μm-wide and 450μm-long push-rod was also measured by loading the lever arm with a 1cm x 75mm x 100μm piece of glass cover slip (~200μN of weight, half of which was supported off-chip). The lever arm was rotated from 60° (when the push-rod is in tension) toward its maximum angle of 140°. The friction force was beyond the fracture limit of the polysilicon force gauge so the friction forces could not be measured. However, the push-rod buckled at roughly 17° past vertical as we rotated the loaded lever arm. This puts the buckling force at approximately 35μN. The calculated values for a 450μm x 15μm x 2μm beam is 19μN if the ends are pinned and 76μN if the ends are fixed. These calculations bracket the measured value of 35μN indicating that our push-rod joints are non-ideal, as expected.

5.5 Additional Measurements

To isolate locations of friction, we have also measured the following additional structures without a load:

- shuttle with shuttle guide
- shuttle without shuttle guide
- shuttle + push-rod + HTB (Fig. 7)
- shuttle + push-rod + lever arm + HTB (Fig. 8).

The mass of our mechanical coupling test structures were estimated to be on the order of a microgram (tens of nanonewtons of force). All structures exhibited roughly the same characteristics shown in Fig. 10 with no significant difference in the measured forces. Clearly, frictional forces dominate over gravitational forces for such light masses. In addition, Figure 12 indicates that friction is not dependent on the mass on the structures but on the adhesive forces between the surfaces[5]. It appears that the coefficient of friction does not apply in the microscale where the weight of the objects are less than the adhesive forces between surfaces.

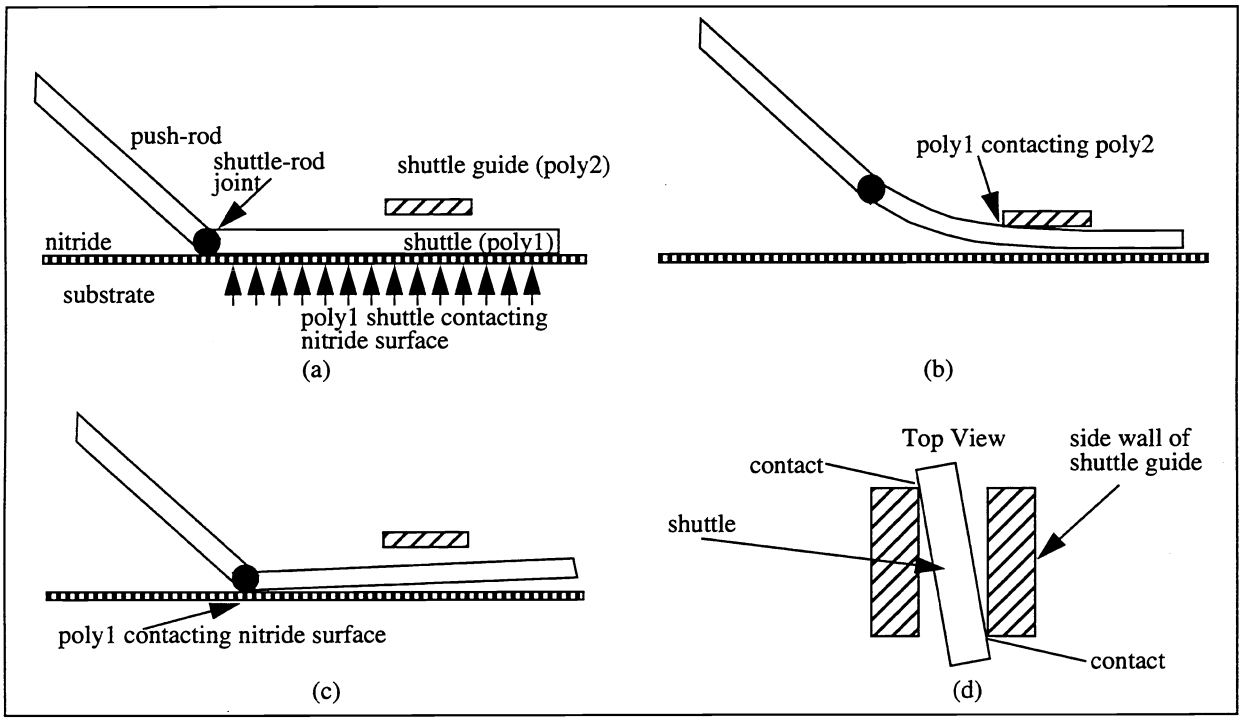

Fig. 13. Sources of friction. (a) The shuttle without a load. The contact force comes from the negligible weight of the shuttle. (b) The shuttle with a load and θ < 90° (push-rod in tension). Notice the shuttle bends upwards and pushes up against the poly 2 shuttle guide. (c) The shuttle with a load and θ > 90° (push-rod in compression). Friction from the shuttle-rod joint being pushed into the nitride surface. (d) The shuttle with or without a load. Skewing of shuttle potentially causes contact between shuttle and the side wall of the shuttle guide.

5.6 Possible sources of friction

Figure 13 shows diagrams of the possible areas of contact between structures for our lever arm system. Figure 13a shows the system without a load. The shuttle rests flatly on the nitride surface due to its weight. When a load is placed on top of the lever arm, the shuttle-rod joint is lifted from the substrate, causing the poly 1 shuttle to bend up and contact the poly 2 shuttle guide designed to keep the shuttle in plane with the substrate (Fig. 13b). The push-rod is in tension in this situation and the friction comes from the shuttle sliding against the shuttle guide (poly 1 to poly 2). As the shuttle is pulled and subsequently the lever arm rotated, there is a transition point where the weight of the payload pushes the push-rod into the nitride surface (Fig. 13c). After this transition, the push-rod is in compression and the friction comes from the shuttle-rod joint sliding against the nitride surface (poly 1 to nitride). In all cases, the shuttle can also be contacting the side walls of the shuttle guide (Fig. 13d), creating more friction. Note that there should be no significant friction from the lever-arm-substrate hinge since its components do not slide against another. Our tests on shuttles with and without a lever arm show no significant difference in the measured forces.

Although the forces measured from a loaded lever arm are roughly an order of magnitude higher those measured for an unloaded lever arm, it is unclear how load mass contributes to the friction in the system. Also, the amount of friction experienced is observed to be spread out over a range of values but the overall trend tends to be higher when the lever arm is near the vertical position. This corresponds to transition between the push-rod in tension (Fig. 13b) and compression (Fig. 13c).

6. DISCUSSION

The data presented above clearly indicates that gravitational forces on these three dimensional polysilicon mechanisms are small compared to forces of friction or adhesion between surfaces. Surface moisture and electrostatic charging have been minimized to some degree, yet there are still unexplained forces present with magnitudes much larger than the weight of the mechanisms and the objects being manipulated. Even more puzzling, these forces do seem to depend on the weight of the applied load.

In the context of building microrobots with multiple degrees of freedom, these measurements indicate that actuator requirements will be in the range of tens to hundreds of micro Newtons of force. In addition, the mechanisms shown require deflections in the hundred micron range to achieve a reasonable workspace. These numbers are consistent with the force and displacement output of linear electrostatic stepper motors[3] with an area of a few tenths of a square millimeter.

7. ACKNOWLEDGMENT

The authors would like to thank Kevin Dang and Richard Liu for building 3-D robot models. All structures shown were fabricated by the ARPA-supported MUMPs process at MCNC. This work was supported in part by NSF and ARPA under award IRI-9321718. Layout and SEM pictures are available through anonymous ftp and http from synergy.icsl.ucla.edu.

8. REFERENCES

1. K. Suzuki, I. Shimoyama, H. Miura, and Y. Ezura, "Creation of an insect-based microrobot with an external skeleton and elastic joints," *IEEE Workshop on Micro Electro Mechanical Systems (MEMS '92)*, pp. 190-195, Travemunde (Germany), 1992.
2. R. Yeh, E.J.J. Kruglick, and K.S.J. Pister, "Towards an articulated silicon microrobot," *ASME Winter Annual Meeting, Micromechanical Systems*, DSC-vol 55-2, pp. 747-754, Chicago, 1994.
3. R. Yeh, E.J.J. Kruglick, and K.S.J. Pister, "Microelectromechanical components for articulated microrobots," *The 8th International Conference on Solid-State Sensors and Actuators (Transducer '95)*, Vol. 2, pp. 346-349, Stockholm (Sweden), 1995.
4. K.S.J. Pister, M.W. Judy, S.R. Burgett, and R.S. Fearing, "Microfabricated hinges," *Sensors and Actuators*, vol. A33, pp. 229-236, 1992.
5. R. Kaneko, "Microtribology related MEMS: concepts, measurements, applications," *Proc. IEEE Workshop on Micro Electro Mechanical Systems (MEMS '91)*, pp. 1-14, Nara (Japan), 1991.
6. S. Suzuki, T. Matsuura, M. Uchizawa, S. Yura, and J. Shibata, "Friction and wear studies on lubricants and materials applicable to MEMS," *Proc. IEEE Workshop on Micro Electro Mechanical Systems (MEMS '91)*, pp. 143-147, Nara (Japan), 1991.

7. K. Noguchi, H. Fujita, M. Suzuki, and N. Yoshimura, "The measurements of friction on micromechatronics elements," *Proc. IEEE Workshop on Micro Electro Mechanical Systems (MEMS '91),* pp. 148-153, Nara (Japan), 1991.
8. M.G. Lim, J.C. Chang, D.P. Schultz, and R.T. Howe, "Polysilicon microstructures to characterize static friction," *Proc. IEEE Micro Electro Mechanical Systems (MEMS '90),* pp. 82-88, Napa Valley, 1990.
9. R. Prasad, N. MacDonald, and D. Taylor, "Micro-Instrumentation for tribological measurement," *The 8th International Conference on Solid-State Sensors and Actuators (Transducer '95)*, Vol. 2, pp. 52-55, Stockholm (Sweden), 1995.
10. G.T. Mulhern, D.S. Soane, and R.T. Howe, "Supercritical Carbon Dioxide Drying of Microstructures," *The 7th International Conference on Solid-State Sensors and Actuators (Transducer '93)*, pp. 296-299, Yokohama (Japan), 1993.